IEEE Robotics and Automation Letters (RA-L) paper, presented at ICRA 2024, Yokohama, Japan. Cite as RA-L paper.

Workstation Suitability Maps: Generating Ergonomic Behaviors on a Population of Virtual Humans with Multi-task Optimization

Jacques Zhong[1,2], Vincent Weistroffer[1], Jean-Baptiste Mouret[2], Francis Colas[2], Pauline Maurice[2]

***Abstract*—In industrial workstations, the morphology of the worker is a key factor for the feasibility and the ergonomics of an activity. Existing digital human modeling tools can simulate different morphologies at work, but hardly scale to a large population of workers because of limited consideration of morphology-specific behaviors and computational cost. This paper presents a framework to efficiently evaluate the suitability of a workstation over a large population of workers in a physics-based simulation. Activities are simulated through a two-step optimization process, involving a quadratic-programming-based whole-body controller and a multi-task optimizer for behavioral adaptation. On a screw-driving scenario, we demonstrate how our framework can help ergonomists improve workstation designs thanks to the resulting suitability maps where generated behaviors are optimized for each morphology w.r.t. ergonomics and performance.**

***Index Terms*—Modeling and simulating humans, human and humanoid motion analysis and synthesis, ergonomics, multi-task optimization**

I. Introduction

MUSCULOSKELETAL disorders (MSD) are a major health issue in industrial workplaces [1]. They compromise the well-being of workers due to chronic body pain and discomfort. Moreover, MSDs are highly prevalent which result in a large scale productivity loss due to absenteeism or presenteeism. Ergonomics assessment aims at identifying high-risk behaviors of workers performing their activity (e.g. awkward postures, high forces, repetitive movements), which then serves to improve workstation designs and thereby reduce MSDs risks.

The risk of developping MSDs depends on individual factors [2] which must be accounted for during the evaluation. One key factor is the morphology which defines the physical characteristics of the worker, including the anthropometric dimensions, the muscular capacities or the endurance limits. For example, small workers have to adopt awkward postures on workstations designed for an average morphology [3]; a high body-mass index (BMI) from obesity correlates with a higher prevalence of MSDs [4]. Thus, workstations need to be designed not for an average-morphology user, but rather by considering the whole population of potential workers. To avoid time-consuming experimental studies, simulation is increasingly used to model and animate humans for ergonomics evaluation during workstation design processes [5] [6] [7]. Simulation has the potential for fully automated assessments with a wide range of indicators [8] in early-stage prototyping of workstations, without needing costly mock-ups or real human data [5] [9]. In this context, a first challenge consists in evaluating if a given morphology is capable of performing an activity in an ergonomic way. Since the human body is highly redundant and able to interact with the environment in various ways, an activity can be performed with various motor behaviors [10]. Yet, the behavior that allows to perform the activity in an ergonomic way may vary depending on the morphology. Therefore, the challenge lies in generating human motions that are optimized w.r.t. the morphology.

Then, since a well-designed workstation should be suitable for a wide range of workers, ergonomics simulation tools should account not only for one or a small number, but for a whole set of different morphologies. Optimizing human whole-body motions even for one morphology is generally computionally expensive [7] [11], and previous works do not

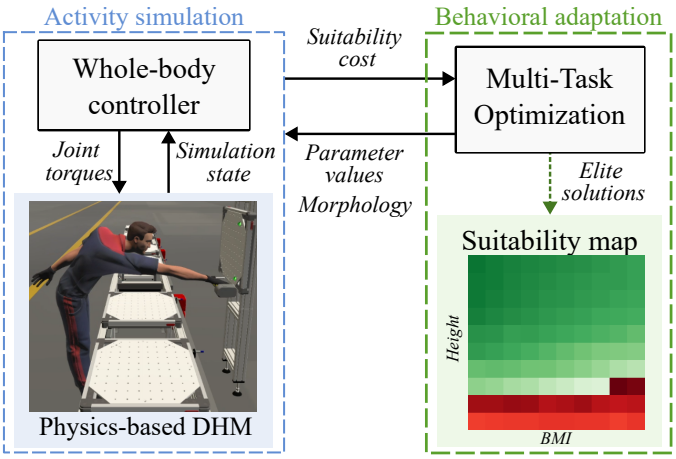

Figure 1: Workflow of the framework. A large population of workers is dynamically simulated using a whole-body controller, and their behaviors are optimized w.r.t. ergonomics using multi-task optimization. The resulting map gives an overview of the workstation suitability for the population.

Manuscript received: Mai, 11, 2023; Revised July, 7, 2023; Accepted September, 11, 2023.

This paper was recommended for publication by Editor A. Kheddar upon evaluation of the Associate Editor and Reviewers' comments. This work was supported by the Continuum project with the use of the Viki XR platform (CEA LIST) and by the French ANR under Grant No. ANR-20-CE33-0004.

[1]J. Zhong and V. Weistroffer are with Université Paris-Saclay, CEA, List, F-91120, Palaiseau, France jacques.zhong@cea.fr, vincent.weistroffer@cea.fr

[2]J. Zhong, J.B. Mouret, F. Colas and P. Maurice are with Université de Lorraine, CNRS, Inria, LORIA, F-54000 Nancy, France pauline.maurice@loria.fr, jean-baptiste.mouret@inria.fr, francis.colas@inria.fr

Digital Object Identifier (DOI): see top of this page.

IEEE Robotics and Automation Letters (RA-L) paper, presented at ICRA 2024, Yokohama, Japan. Cite as RA-L paper.

IEEE Robotics and Automation Letters (RA-L) paper, presented at ICRA 2024, Yokohama, Japan. Cite as RA-L paper.

address the scalability issue when a large number of morphologies need to be simulated [9] [12]. Therefore, a second challenge is to account for a large number of morphologies in a computationally-efficient way.

This paper thus aims at developing a framework that allows to assess the suitability of a workstation for a large population of morphologically distinct workers. To address the aforementioned challenges, i.e. generation of morphology-specific behaviors and computational efficiency over large morphology sets, the paper proposes the following contributions:

- A framework that efficiently generates morphology-specific optimal behaviors w.r.t. ergonomics and activity performance, for a large number of morphologies.
- A global visualization of the workstation suitability over a large population of workers through **suitability maps**.
- An example application of the proposed framework on a screwdriving activity as a proof of concept.

The proposed approach combines a whole-body controller (WBC) [13] in a physics engine to simulate the activity on a variety of morphologies (section III-B) with a multi-task optimization algorithm (Multi-Task MAP-Elites [14]) to explore controller configurations and generate behaviors adapted to each morphology (section III-C) (Figure 1). The framework is demonstrated on a screw-driving activity (section IV), to both show how it can help studying workstation suitability and behavioral strategies over a large population, and benchmark its computational efficiency (section V).

II. Related works

A. Ergonomics evaluation

Traditionnally, ergonomists use pen-and-paper methods to quantify MSDs risk by observing workers performing the activity [8]. The indicators used typically consist in a scoring system implementing guidelines from epidemiological studies, in terms of postures, repetitiveness or load values. But these indicators use rough threshold values and are posture-based with limited considerations for dynamical effects.

Recent works focus on simplifying the ergonomics assessment process towards non-expert users. Using motion capture, many frameworks can automatically compute a variety of ergonomics indicators, e.g. continuous RULA [15] or biomechanical-based indicators accounting for dynamical effects (e.g. joint torques, whole-body stability) [9]. Application ranges from online ergonomics assessment [16] to adaptive cobotic assistance based on estimating the overloading torques [17]. Virtual or augmented reality has also been used to reduce the need for costly physical workstations mock-ups in ergonomics studies [18]. However, these frameworks still require real human data, which can be complex and costly to obtain especially when studying a large population of workers.

B. DHM software and whole-body animation

Digital Human Models (DHM) can be used to simulate the human body and replace human data. With ergonomics-oriented DHM software (e.g. Jack [5] [6]), entire workstations can be designed and simulated without the need for physical protoypes or motion capture sessions. Various virtual workers can be created using anthropometric databases [19] or statistical models from multivariate anthropometrics [20]. Virtual workers are then animated to perform activities, using pre-recorded animations or inverse-kinematics (IK) techniques based on user-defined target poses. As discussed in [9], such animation methods neglect the dynamical effects of body segments or external loads, which have an impact especially for outlying morphologies (e.g. high stature, high BMI). In [6], terms are added in the IK problem to generate motions that account for external loads and interal efforts minimization, but only the equations of statics are considered. Overall, these kinematic-based methods lead to unrealistic whole-body motions and inaccurate estimations of the internal body efforts.

C. Physics-based DHM

To overcome the limitations of kinematic-based methods, dynamically simulated DHMs are needed. Musculoskeletal DHMs (e.g. Anybody [7]) can be dynamically simulated to model detailed biomechanical effects within the human body. However, these models are computationally expensive, especially when it comes to forward dynamics simulation.

An emerging approach in ergonomics consists in simulating joint-actuated DHMs (i.e. no muscles) in a physics engine with WBC [21] [9]. WBC are used in humanoid robotics for real-time computation of optimal joint torques w.r.t user-defined tasks and constraints [13] [22]. In [21] [9], a WBC is used for generating dynamically consistent DHM motions and estimating internal efforts, which paves the way for dynamic-based ergonomics assessments. However, the parameters of a WBC must be fine-tuned for each activity and human morphology, which involves a complex black-box problem usually solved with evolutionary algorithms [11] [12] or Bayesian optimization with dimensionality reduction [23]. In previous ergonomics-centered works with several human morphologies, this problem has either been ignored [9] or solved separately for each morphology [12], which becomes prohibitively costly when a large population is considered.

Deep reinforcement learning controllers are another promising approach, with virtual characters able to reproduce highly dynamical motions from motion capture inputs [24]. In [25], the control policy learns the dynamical effects of anthropometric dimensions allowing for real-time gait retargeting to a continuous space of morphologies. However, these approaches have a high training cost and a limited configurability with policies highly overfitted over the reference motions.

Our goal is to assess the suitability of a workstation for a large population of workers. Our approach uses joint-actuated DHMs with a WBC, which parameters are optimized w.r.t. ergonomics to generate morphology-specific behaviors. To avoid solving this problem from scratch for each morphology, we use a multi-task optimizer which leverages solutions from other morphologies to significantly reduce the simulation cost.

III. Methods

The proposed framework consists in two levels of optimization (Figure 1). In the *activity simulation* part (section III-B),

IEEE Robotics and Automation Letters (RA-L) paper, presented at ICRA 2024, Yokohama, Japan. Cite as RA-L paper.

the physics-based DHM is animated using optimal joint torques computed by a whole-body controller. In the *behavior adaptation* part (section III-C), the controller parameters are optimized for each morphology with a multi-task algorithm.

A. Problem statement

The problem consists in assessing the suitability of a workstation activity a for a population of workers $\mathcal{M}$. The workstation is suitable for a worker if the worker is able to complete the activity in an ergonomic way. The same activity a can be performed using many different whole-body motions [10]. To account for this variability, the set of possible motor behaviors for a worker $m \in \mathcal{M}$ is denoted ${}_a\mathcal{B}^m$. We note ${}_a f^m_{\text{suit}}$ (noted f_{suit} later on to simplify notation) a measure of the suitability of activity a for the morphology m. The following multi-task optimization (MTO) problem is solved:

$$\forall m \in \mathcal{M} \quad \arg\min_{b \in {}_a\mathcal{B}^m} \; {}_a f^m_{\text{suit}}(b) \tag{1}$$

B. Activity simulation

1) Digital human model: The DHM is composed of 21 rigid bodies linked by 20 joints, for a total of 47 internal DoFs modeled as actuated revolute joints, and 6 additional non-actuated DoFs from the floating base. Joint-actuated human models involve lower computational costs compared to musculoskeletal models [7], which is crucial when a large number of simulations are needed. The DHM is implemented in the XDE physics engine [26] with the Unity platform.

Different morphologies can be generated by specifying the height and the BMI of the DHM. The dimensions and inertial properties of the body segments are automatically scaled according to average anthropometric coefficients as in [18]. The joint torques capacities $\tau_{\max}$ (maximum torque each joint can produce) are scaled with respect to the BMI and height. $\tau_{\max}$ changes linearly with respect to the BMI, based on the muscular strength in obese and non-obese populations from comparative studies [27] [28] [9]. Then, for a given BMI, $\tau_{\max}$ scales linearly with respect to the height by assuming that the proportion of fat-free mass is constant for a given BMI.

2) QP control: Dynamically-consistent DHM motions are generated with a whole-body controller based on quadratic programming (QP) as in [13] [9]. At each simulation step, the QP controller computes the optimal joint torques allowing the DHM to perform various tasks (e.g. track hand trajectories, maintain balance) under physical (e.g. contact conditions) and biomechanical (e.g. joint limits) constraints, by solving the following convex optimization problem:

$$\arg\min_{\chi=(\tau,f_c)} \quad \sum_{i=0}^{n_{\text{task}}} w_i \left\| A_i\chi - a_i \right\|^2 \tag{2a}$$

$$\text{s.t.} \quad C_{in}\chi \leq c_{in} \tag{2b}$$

$$C_{eq}\chi = c_{eq} \tag{2c}$$

$$M\dot{\nu} + h = S\tau + \sum_{k=0}^{n_{\text{contact}}} J_{c_k}^T f_{c_k} \tag{2d}$$

with:

- $\chi = (\tau, f_c)$ the optimization variables, with τ the joint torques and f_c the body/environment contact wrenches.
- QP tasks (Equation 2a) defined as errors between a current and a desired acceleration or force, in the Cartesian or joint space, where (A_i, a_i) serve to express tasks in the optimization variables χ (see [13]). w_i defines the weight (i.e. priority) of the i-th task among n_{task} tasks.
- $(C_{eq},\ c_{eq})$ and $(C_{in},\ c_{in})$ implement respectively the equality and inequality constraints corresponding to the planar contact constraints (feet/ground non sliding contact conditions, always active in this work since we focus on activities without locomotion) and the joint limit constraints (velocities, accelerations, torques) that implements biomechanical limits of the human body.
- The equation of motion as constraint for dynamic consistency (Equation 2d), with M the mass matrix, ν the generalized velocities, h the Coriolis, centripetal and gravity terms, S the selection matrix and f_{c_k} the wrench at the k-th contact point with J_{c_k} the corresponding Jacobian matrix.

3) QP tasks: The QP problem uses the following set of tasks that are generic enough to allow the simulation of various human manual activites (as in [12]):

- Cartesian(s) task(s) on the hand frame(s), where the reference (i.e. desired) trajectories are activity-specific.
- A head orientation task directed at the hand frame, such that the worker looks at what he is doing.
- A center of mass (CoM) task to maintain balance.
- Postural (i.e. joint position) tasks on the torso, left arm, right arm, neck and legs to favor the motion of certain joints compared to others, and thereby generate different behaviors by changing the relative tuning of these tasks. The postural tasks reference is the standing neutral posture (N-pose) as in REBA [8]
- A torque minimization task to avoid excessive internal efforts associated with higher risks of MSDs

The tasks and constraints are either defined in the Cartesian space (thus independent of the morphology) or automatically rescaled with respect to the morphology (as with the joint torque limits). In this work, the QP problem is implemented using the open-source TSID (Task Space Inverse Dynamics) library [22] [1].

C. Behavioral adaptation

1) Multi-task MAP-Elites: Multi-task MAP-Elites (MTME) [14] is an evolutionary algorithm dedicated to efficiently find high-performing solutions for many different but related tasks (i.e. problems). The main intuition is that similar problems have similar solutions. Instead of optimizing each problem separately, MTME keeps the best solution (*elite*) for each problem in an archive and iteratively combines these elites with genetic operators in order to improve the archive. In our MTO problem (see section III-A), each task (in the sense of MTME) corresponds to the behavior optimization problem for one morphology. A simplified pseudo-code of MTME (Alg. 1)

[1] Source code: https://github.com/stack-of-tasks/tsid

IEEE Robotics and Automation Letters (RA-L) paper, presented at ICRA 2024, Yokohama, Japan. Cite as RA-L paper.

highlights the main steps of the algorithm. The open-source reference implementation in Python [14] was used [2].

Algorithm 1 Multi-task MAP-Elites [14] simplified pseudo-code, applied to our problem.

```
Archive ← Generate and evaluate random solutions
for K evaluations do
  x ← Generate a solution from two elites in Archive
  m ← Select a morphology in 𝓜
  b ← Simulate activity with solution x on morphology m
  if f_suit(b) < Archive(m) then
    Archive(m) = f_suit(b)
  end if
end for
```

2) Morphology space: The morphology space is a set of DHMs with different morphological characteristics. In general, relevant dimensions should be chosen according to the study e.g. height, BMI, body length ratios.

3) Search space: The search space is the set of parameters influencing the human motor behavior and optimized by MTME. The parameters should be chosen so that they have a significant impact on the motor behavior of the DHMs (e.g. task parameters of the WBC, DHM feet placement).

4) Suitability cost: The objective is to find, for each morphology, a behavior allowing to complete the workstation activity in the most ergonomic way. To guide the optimization process, three cases are considered in the suitability cost f_{suit}:

$$f_{\text{suit}} = \begin{cases} p_1 & \text{if early termination} \quad (3a) \\ f_{\text{perf}} + p_2 & \text{if } C_{\text{perf}} \text{ false} \quad (3b) \\ f_{\text{ergo}} & \text{if } C_{\text{perf}} \text{ true} \quad (3c) \end{cases}$$

If the activity is not completed at all (Equation 3a) (early termination, e.g. the worker falls or is unable to grab a necessary tool), the cost function is assigned a high penalty p_1 in order to dismiss the solution. If the activity is executed until the end, the quality of execution is measured with the performance cost f_{perf} (e.g. accuracy or rapidity), and compared to the activity performance requirements C_{perf} (the definition of f_{perf} and C_{perf} is activity-specific, see section IV). If C_{perf} are not satisfied (Equation 3b), the cost function is the task performance metrics f_{perf}, plus a small penalty term p_2 to reduce the relevance of this solution. If C_{perf} are satisfied (Equation 3c), then the cost function is an ergonomic cost f_{ergo} that evaluates MSDs risk. This means the ergonomics of the motion is considered only when the activity is completed satisfactorily (the feasibility is prioritized over the ergonomics).

In this work, we define the ergonomic cost f_{ergo} as the normalized torques averaged over the joints and the simulation steps [9] (but it could be replaced by other ergonomic scores):

$$f_{\text{ergo}} = \frac{1}{T}\sum_{t=0}^{T}\left[\frac{1}{N}\sum_{n=0}^{N}\left[\max_{i}\left(\frac{|\tau_{n,i}(t)|}{\tau_{n,i}^{\max}}\right)\right]\right] \quad (4)$$

with T the total simulation timesteps, N the number of joint, $\tau_{n,i}$ the i-th DoF of the n-th joint and $\tau_{n,i}^{\max}$ the maximum exertable torque of the DoF. This indicator estimates the overall stress applied on the joints during the whole activity, on a scale from 0 (no stress at all) to 1 (maximum stress on all joints).

[2]Source code: https://github.com/resibots/pymap_elites

IV. Experiments

We now demonstrate our framework on an example screw-driving activity as a proof of concept.

A. Screw-driving activity

The activity consists in a simulated assembly line screw-driving activity. The activity starts with the simulated human in the N-pose and pre-defined feet positions. The human then grabs an electric screwdriver ($2\,\text{kg}$) with his right hand, and reaches forward to two points located on a panel above a conveyor belt, staying $2\,s$ on each point to simulate setting screws. The whole activity lasts around $10\,s$. A conveyor belt ($75\,\text{cm}$ high) is positioned between the worker and the panel, and the worker cannot lean on it.

The activity is simulated using the QP tasks defined in section III-B3, where a reference trajectory for the right hand Cartesian task is computed from the target waypoints interpolated with a minimum-jerk polynomial. The only contacts included in the QP formulation are the fixed feet/ground contacts. The activity terminates early if the DHM falls, cannot reach the tool, or if a lower-body segment collides with the conveyor belt.

Since our framework is meant to help designers iteratively improve workstation designs to accomodate a large population of workers, we present two variants of the example activity, which represent the iterative design process:

- Scenario A: the conveyor belt is $100\,\text{cm}$ wide.
- Scenario B: the conveyor belt is $80\,\text{cm}$ wide.

We expect scenario A (initial design) to be less suitable than scenario B (improved design), especially for smaller morphologies with limited reaching capabilities.

B. Activity-specific formulation

1) Morphology space: Each morphology is defined by a height and a BMI. The whole space consists in 10 heights (from $1.5\,\text{m}$ to $1.95\,\text{m}$) and 10 BMIs (from 16 - underweight to 34 - obese) both equally spaced, for a total of 100 different morphologies.

2) Search space: The search space contains 10 parameters (Table I) that were manually selected, based on pilot tests in simulation on outlying morphologies:

- The weights ($w_{\text{p,torso}}$, $w_{\text{p,leg}}$, $w_{\tau_{\text{min}}}$) and gains (used for position servoing [13]) (K_{c}, K_{p}) of the QP tasks.
- The reference position $x_{\text{com}}^{\text{ref}}$ of the CoM task along the anterior-posterior axis. To ensure the reference CoM does not lie outside the support polygon, $x_{\text{com}}^{\text{ref}}$ is normalized with respect to the limits of the polygon of support.
- The feet positions in the horizontal ground plane, with (δx_{ft}, δy_{ft}) the feet spacing and (x_{root}, y_{root}) the position of the midpoint of the segment connecting the two feet expressed w.r.t. the origin frame.

IEEE Robotics and Automation Letters (RA-L) paper, presented at ICRA 2024, Yokohama, Japan. Cite as RA-L paper.

Table I: Values of the WBC parameters. The parameters optimized with MTME and their search intervals are in bold.

Parameters		Value(s)	Parameters		Value(s)
Postural tasks			*CoM task*		
· **Gain**	$\boldsymbol{K_p}$	**[250;2500]**	· Gain		200
· **Legs weight**	$\boldsymbol{w_{p,leg}}$	**[1;100]**	· Weight		1e5
· **Torso weight**	$\boldsymbol{w_{p,torso}}$	**[1;100]**	· **Reference (X)**	$\boldsymbol{x_{com}^{ref}}$	**[-0.5;0.8]**
· Neck weight		0.01			
· Left arm weight		1	*Torque min. task*		
· Right arm weight		0.001	· **Weight**	$\boldsymbol{w_{\tau_{min}}}$	**[0.1;10]**
Cartesian tasks			*Feet positioning*		
· **Hand gain**	$\boldsymbol{K_c}$	**[1e3;1e4]**	· **X spacing**	$\boldsymbol{\delta x_{ft}}$	**[-0.4;0.4]**
· Hand weight		100	· **Y spacing**	$\boldsymbol{\delta x_{ft}}$	**[0.1;0.6]**
· Head gain		500	· **X root**	$\boldsymbol{x_{root}}$	**[-0.4;0.4]**
· Head weight		100	· **Y root**	$\boldsymbol{y_{root}}$	**[0.1;0.6]**

3) Performance cost: The activity is performed successfully if the DHM brings the screwdriver within a threshold to the targets. We define the activity performance conditions $\mathcal{C}_{perf}$ as:

$$\mathcal{C}_{perf} = \begin{cases} \epsilon_p \ \leq \ \epsilon_p^* = 0.05m \\ \epsilon_r \ \leq \ \epsilon_r^* = 10^\circ \end{cases} \tag{5}$$

with ϵ_p and ϵ_r respectively the position and orientation errors (angle between the screwdriver axis and the hole normal axis), averaged over the timesteps when the tool is expected to be on a target. ϵ_p^* and ϵ_r^* are respectively the position and orientation error thresholds allowed for the activity. The activity performance cost f_{perf} (Equation 3b) is defined as:

$$f_{perf} = \frac{1}{2}\left(\max\left(0, \frac{\epsilon_p - \epsilon_p^*}{\epsilon_p^*}\right) + \max\left(0, \frac{\epsilon_r - \epsilon_r^*}{\epsilon_r^*}\right)\right) \tag{6}$$

In Equation 3, we use $p_1 = 2000$, $p_2 = 1000$ to ensure a strong hierarchy between the three cases.

C. Simulation runs

We ran the framework with MTME on both scenarios A and B for 50000 evaluations (10 runs), which was enough to observe a low frequency of updates in the archive of elites ($< 5\%$) at which we considered the convergence sufficient. The results presented in section V-A and V-B are based on the median run in terms of the average value of f_{suit} over all morphologies. MTME was also benchmarked against three other algorithms on scenario A to evaluate its computational efficiency (section V-C). In this case, the algorithms were all compared at 30000 evaluations (10 runs each):

- *Random*: at each evaluation, a random behavior is evaluatued for a random morphology. As with MTME, the elite solution of each morphology is kept in an array.
- *CMA-single*: the behavior is optimized for each morphology separately with CMA-ES, a state-of-the-art black-box optimizer (classic way of solving a MTO problem with single-task optimization) [29]. To keep the evaluation budget constant, each morphology is evaluated 300 times.
- *CMA-all*: to verify if MTO is needed, we look for one same optimal solution for all morphologies. Each solution is evaluated over the entire population, and the average f_{suit} over all morphologies is optimized with CMA-ES.

We define the fail rate as the proportion of morphologies unable to complete the activity. To estimate the minimum achievable fail rate, the morphologies not satisfying C_{perf} on the MTME runs are optimized with CMA-ES with a larger budget (10000 evaluations each, 5 runs). The fail rate is a decent approximation of the average suitability cost, as the penalty terms dominate f_{suit} if the activity is not completed.

Each run was launched on a computing cluster with a 32 cores CPU (Intel Xeon E5-2620 v4). A run of 30000 evaluations took approximately 5 days regardless of the algorithm.

V. Results

A. Workstation suitability

The suitability of a scenario for the considered population is evaluated using the suitability scores f_{suit} of all morphologies. $\mathcal{M}_{p+}$ (resp. $\mathcal{M}_{p-}$) is defined as the set of morphologies that match (resp. do not match) the performance conditions C_{perf} (Equation 3a - Equation 3c). A scenario is considered suitable if all the morphologies belong to $\mathcal{M}_{p+}$.

Scenario A: Figure 2 displays the suitability map – i.e. the suitability scores across morphologies – for scenario A. For the sake of readability, the map shows only the performance cost f_{perf} (see Equation 3b) for morphologies in $\mathcal{M}_{p-}$ (red colors on the map), rather than the full value of f_{suit}. For morphologies in $\mathcal{M}_{p+}$, f_{suit} equals to f_{ergo} (see Equation 3c) so the map displays the ergonomic cost (green colors).

Twenty-two out of 100 morphologies belong to $\mathcal{M}_{p-}$. The suitability of the workstation is mainly affected by the DHM height: Morphologies smaller than 1.6 m all belong to $\mathcal{M}_{p-}$, while morphologies taller than 1.6 all belong to $\mathcal{M}_{p+}$. In addition, within $\mathcal{M}_{p-}$ the performance cost averaged over same height morphologies f_{perf}^H improves with height: f_{perf}^H ranges from 0.805 for H = 1.5 m to 0.058 for H = 1.6 m (the lower f_{perf} the better). Within $\mathcal{M}_{p+}$, the ergonomic cost f_{ergo} improves (i.e. decreases) with increasing height. This height-dependency is expected, as tall people can reach farther without having to bent forward. **Therefore, scenario A is not suited to the entirety of the studied population.**

Scenario B: The suitability map for scenario B (Figure 3) only displays the ergonomic cost f_{ergo}, as all morphologies are able to perform the task (i.e. belong to $\mathcal{M}_{p+}$). The average f_{ergo} over $\mathcal{M}_{p+}$ is better in Scenario B (0.070 ± 0.010) than in scenario A (0.117 ± 0.026). The dispersion of the f_{ergo} values is lower in scenario B, which indicates a more homogeneous ergonomic cost over the population. This is consistent with the conveyor belt being less wide, which enables workers to move closer to targets while having to bend forward less. **Therefore, scenario B is better suited to the whole considered population thanks to the reduced width on the conveyor belt.**

The attached video shows the generated motions for a few morphologies for both scenarios.

B. Behavioral strategies

This part presents an in-depth analysis of scenario A for which a higher variability on f_{suit} was observed.

IEEE Robotics and Automation Letters (RA-L) paper, presented at ICRA 2024, Yokohama, Japan. Cite as RA-L paper.

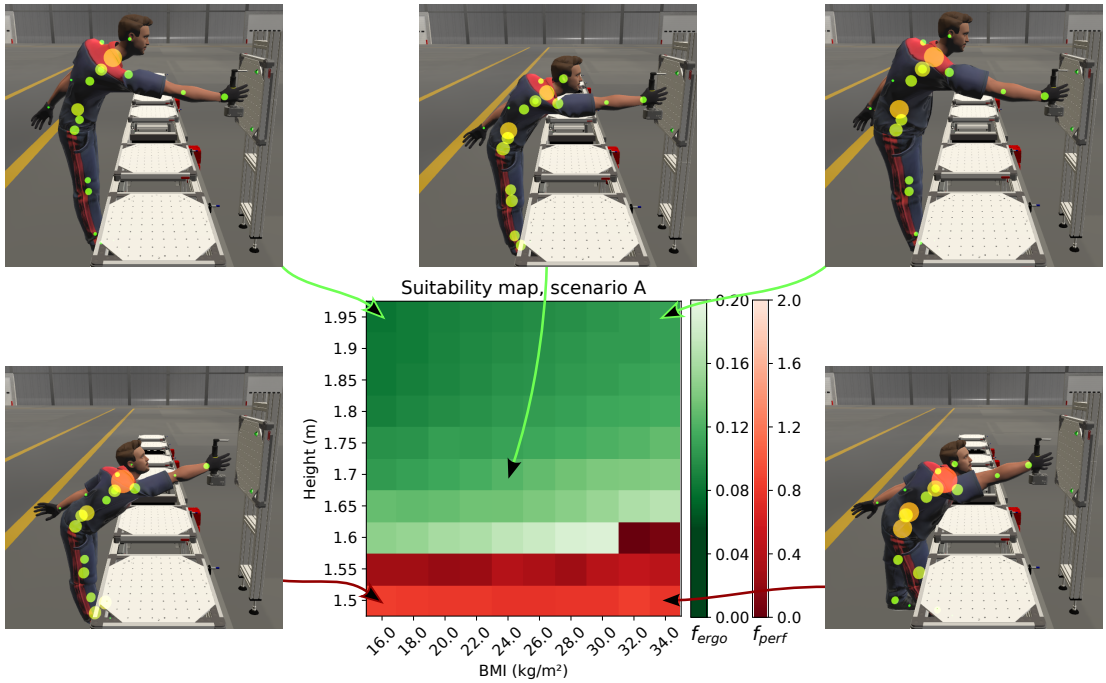

Figure 2: Suitability map for scenario A and screenshots of example morphologies setting the screw on the second point. The map shows the performance cost f_{perf} if C_{perf} is not matched (red colors) and the ergonomic cost f_{ergo} otherwise (green colors). On the screenshots, the colored spheres represent the instantaneous normalized joint torques (green: low, red: high).

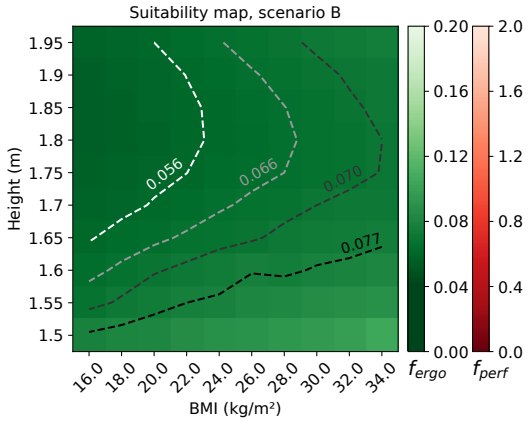

Figure 3: Suitability map for scenario B. Each contour line delimits a percentile of the f_{ergo} values, from the 20$^{\text{th}}$ (white line) to the 80$^{\text{th}}$ (black line).

Effect of height: Figure 2 displays example morphologies performing the activity. Small workers adopt awkward postures in terms of ergonomics, with the back strongly bent and the right shoulder raised. Indeed, the back flexion angle is higher across the whole activity execution for small morphologies compared to taller ones (Figure 4a): the maximum back flexion angle is 67 ° for a 1.5 m tall DHM compared to 35 ° for a 1.95 m tall DHM. Figure 4b depicts the CoM stability margin across time for various DHM heights. Here, the CoM stability margin defines the distance between the CoM and the front limit of the support polygon, projected on the horizontal plane. Overall, this margin decreases with the height. In addition, while the margin is almost constant across the whole activity execution for morphologies in $\mathcal{M}_{p+}$, it decreases with time for morphologies in $\mathcal{M}_{p-}$ (H = 1.5 m and H = 1.55 m). Small workers need to bend forward further than taller ones to reach the target points, which leads to less stable and overall less ergonomic postures.

Effect of BMI: According to the suitability map (Figure 2), within $\mathcal{M}_{p+}$ the ergonomic cost f_{ergo} gets worse (increases) with increasing BMI. The ergonomic cost averaged over same BMI morphologies $f_{\text{ergo}}^{\text{BMI}}$ ranges from 0.096 (i.e. 9.6% of maximum torque capacity) for BMI = 16 (underweight population) to 0.126 (12.6% of maximum torque capacity) for BMI = 34 (overweight population). Contrary to the height, the back flexion angle is not significantly affected by the BMI (Figure 4c). However, higher BMIs results in higher joint torques especially on the lumbar joints (Figure 4d) and the lower-body joints. The effect of BMI on lumbar torque is particularly significant from 3 seconds onwards, after the DHM grabs the tool and starts bending forward. This result is consistent with the fact that overweight people usually have a lower strength to body mass ratio compared to average BMI people [28]. With the increase of mass (and the associated inertial effects), reaching for extreme postures while maintaining balance becomes more difficult.

Behavior variability: Figure 5a shows the value distribution for each optimized parameter (see Table I) over the elites solutions. These distributions are multimodal which means that MTME converges to morphology-specific behaviors (i.e. different optimal behaviors for different morphologies). Figure 5 displays maps of optimal parameter values over morphologies, for 4 parameters. The torso and legs postural weights (resp. $w_{\text{p,torso}}$, $w_{\text{p,leg}}$) are lower for small morphologies (resp. Figure 5b and Figure 5c). With lower postural weights, the DHM is able to reach a posture farther from the reference neutral posture, which is needed for smaller DHMs to reach

IEEE Robotics and Automation Letters (RA-L) paper, presented at ICRA 2024, Yokohama, Japan. Cite as RA-L paper.

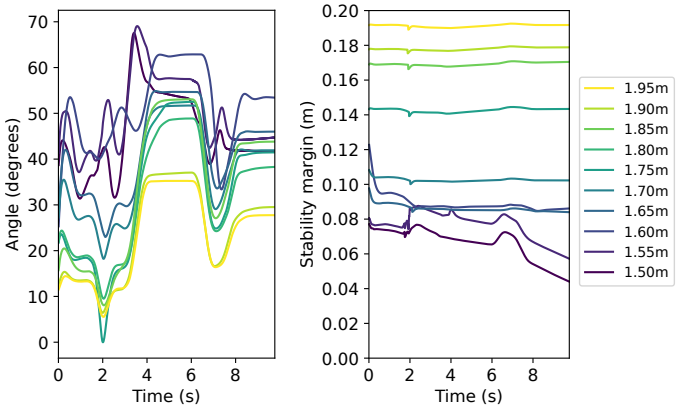

(a) Back angle (BMI=24) (b) CoM stability margin (BMI=24)

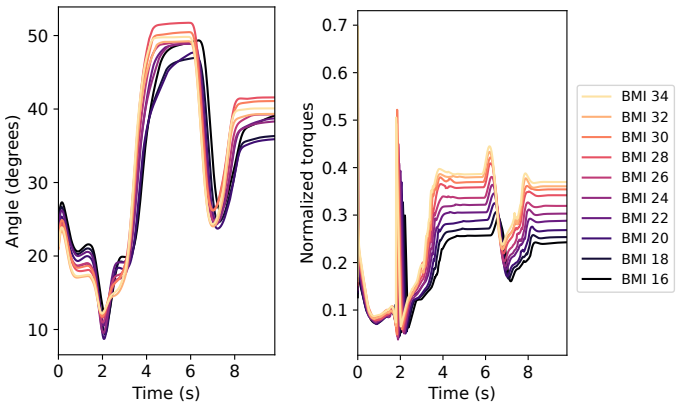

(c) Back angle (H=1.8 m) (d) Normalized lumbar torques (H=1.8 m)

Figure 4: Time-series of 4 different kinematic and dynamic quantities for scenario A. The back flexion angle is measured from the vertical axis to the projection of the pelvis-neck line on the sagittal plane, as in REBA [8]. Lumbar torques are normalized w.r.t. the torques capacities of each morphology.

the targets. Similarly, the CoM reference $x_{\text{com}}^{\text{ref}}$ is higher for smaller morphologies (Figure 5d), which is helpful for them to bend further forward. Moreover, the torque minimization weight $w_{\tau_{\text{min}}}$ is lower on taller and heavier morphologies (Figure 5e). For these morphologies, higher absolute joint torques are needed to perform the activity, which requires a lower weight for the torque regularization task.

C. Baseline comparisons

The evolution of the fail rate for MTME and the 3 baseline algorithms is displayed on Figure 6. At 30000 evaluations, *CMA-all* has the highest median fail rate (0.58) and performs even worse than *Random* (0.5). With *CMA-all*, the problem is optimized as a single-task problem (i.e. one solution for all morphologies). This shows the necessity of optimizing for each morphology individually in a multi-task context.

At 30000 evaluations, MTME outperforms all the baselines with a median fail rate (0.22) lower than that of *CMA-single* (0.4) and *Random* (0.5). MTME shows some variability with a fail rate difference of 0.11 between the worst run and the best run; the worst run still outperforms the best run of any baselines. Moreover, MTME reaches the final fail rate of *CMA-single* 6.5 times earlier and that of *Random* 14

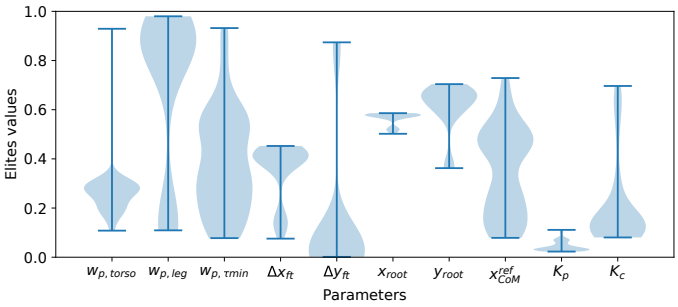

(a) Parameter values over elite solutions.

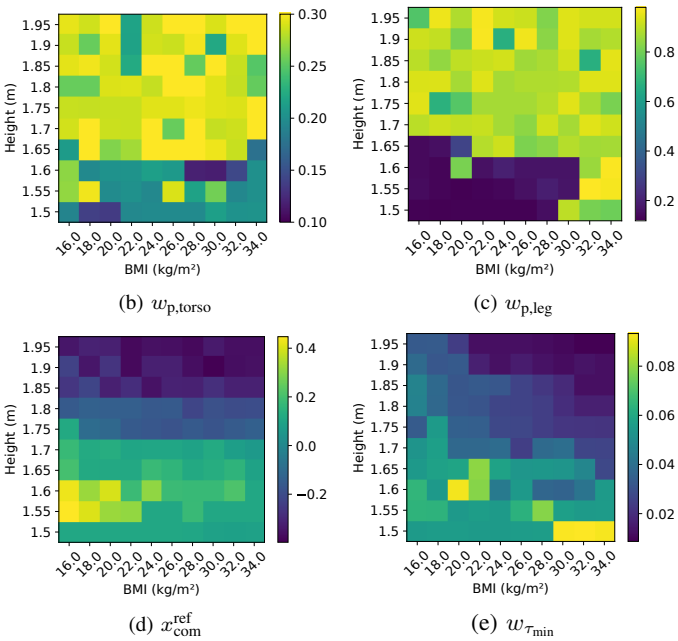

(b) $w_{\text{p,torso}}$ (c) $w_{\text{p,leg}}$

(d) $x_{\text{com}}^{\text{ref}}$ (e) $w_{\tau_{\text{min}}}$

Figure 5: **(a)** Distributions of the optimized parameters over the elite solutions, normalized w.r.t. the search space intervals. **(b) - (e)** Maps of optimized parameter values over the morphology space.

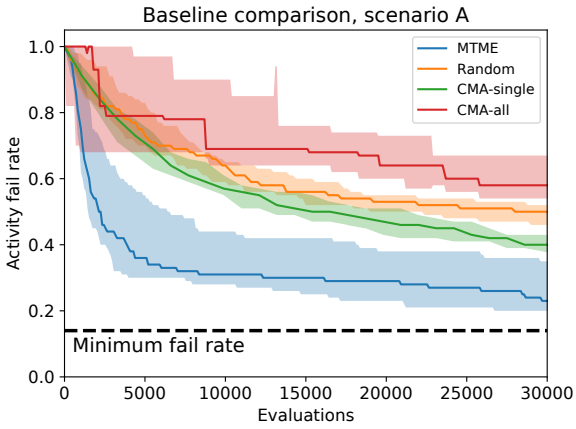

Figure 6: Evolution of the activity fail rate for MTME and three baselines (CMA-single, Random and CMA-all). The solid line shows the median fail rate while the shaded regions shows the minimum and maximum fail rates.

IEEE Robotics and Automation Letters (RA-L) paper, presented at ICRA 2024, Yokohama, Japan. Cite as RA-L paper.

times earlier. This demonstrates the pertinence of using multi-task optimization through MTME as similar morphologies are expected to have similar solutions.

The attached video shows the best behavior generated by each baseline on an average DHM (H=1.7, BMI=24). At 30000 evaluations, the activity is completed only with MTME and CMA-single, with MTME having a better (i.e. lower) suitability cost f_{suit}.

VI. Conclusion

The paper presented a framework to study workstation suitability for large populations of workers, by combining whole-body control and multi-task optimization. On an example screw-driving scenario with 100 different morphologies, our framework generated ergonomically-optimized behaviors for each morphology, and a suitability map over the population. This can help a designer to identify a poorly designed workstation and improve it based on the suitability and behavioral analysis. Moreover, we showed that Multi-Task MAP-Elites reduces the simulation cost when many morphologies are considered, compared to other state-of-the-art approaches.

Currently, the whole problem is optimized from scratch when the workstation or the set of morphology changes. Future work will explore the transfer of optimized solutions to resembling scenarios or morphological spaces to further reduce computational costs. Moreover, some generated motions are not yet fully human-like, because of some current limitations of our WBC (a real human might find a better solution). Yet, this could be improved by various additions to the controller without affecting the MTME part. For example, this includes considering multi-contact dynamics (e.g. hand or legs against the conveyor belt), handling self-collisions (as in [30]) or optimizing the reference trajectories directly (as in [12]) or with planning. Future studies will be directed towards assessing the usability and the validity of the proposed framework with ergonomists on various scenarios involving real human data.

References

[1] S. Bevan, "Economic impact of musculoskeletal disorders (MSDs) on work in Europe," *Best Practice and Research: Clinical Rheumatology*, vol. 29, no. 3, pp. 356–373, 2015.

[2] D. C. Cole and I. Rivilis, "Individual factors and musculoskeletal disorders: a framework for their consideration," *J. of Electromyography and Kinesiology*, vol. 14, no. 1, pp. 121–127, 2004.

[3] D. B. Chaffin, J. J. Faraway, X. Zhang, and C. Woolley, "Stature, Age, and Gender Effects on Reach Motion Postures," *Human Factors*, vol. 42, no. 3, pp. 408–420, 2000.

[4] P. Buckle and J. Buckle, "Obesity, ergonomics and public health," *Perspectives in Public Health*, vol. 131, no. 4, pp. 170–176, 2011.

[5] U. Raschke and C. Cort, "Siemens Jack," in *DHM and Posturography*, S. Scataglini and G. Paul, Eds. Academic Press, 2019, pp. 35–48.

[6] K. Abdel-Malek, J. Arora, R. Bhatt, K. Farrell, C. Murphy, and K. Kregel, "Santos: An integrated human modeling and simulation platform," in *DHM and Posturography*, S. Scataglini and G. Paul, Eds. Academic Press, 2019, pp. 63–77.

[7] M. Damsgaard, J. Rasmussen, S. T. Christensen, E. Surma, and M. de Zee, "Analysis of musculoskeletal systems in the AnyBody Modeling System," *Simulation Modelling Practice and Theory*, vol. 14, no. 8, pp. 1100–1111, 2006.

[8] S. Hignett and L. McAtamney, "Rapid Entire Body Assessment," *Applied Ergonomics*, vol. 31, pp. 201–205, 2000.

[9] P. Maurice, V. Padois, Y. Measson, and P. Bidaud, "Human-oriented design of collaborative robots," *International Journal of Industrial Ergonomics*, vol. 57, pp. 88–102, 2017.

[10] D. Srinivasan and S. E. Mathiassen, "Motor variability in occupational health and performance," *Clinical Biomechanics*, vol. 27, no. 10, pp. 979–993, 2012.

[11] L. Penco, E. M. Hoffman, V. Modugno, W. Gomes, J. B. Mouret, and S. Ivaldi, "Learning Robust Task Priorities and Gains for Control of Redundant Robots," *IEEE Rob. and Autom. Let.*, vol. 5, no. 2, 2020.

[12] W. Gomes, P. Maurice, E. Dalin, J.-B. Mouret, and S. Ivaldi, "Multi-Objective Trajectory Optimization to Improve Ergonomics in Human Motion," *IEEE Rob. and Autom. Let.*, vol. 7, no. 1, pp. 342–349, 2022.

[13] J. Salini, V. Padois, and P. Bidaud, "Synthesis of complex humanoid whole-body behavior: A focus on sequencing and tasks transitions," *Proceedings - IEEE Int. Conf. Rob. and Autom.*, pp. 1283–1290, 2011.

[14] J.-B. Mouret and G. Maguire, "Quality Diversity for Multi-task Optimization," in *Proceedings of the 2020 Genetic and Evolutionary Computation Conference*, 2020, pp. 121–129.

[15] A. Yazdani, R. S. Novin, A. Merryweather, and T. Hermans, "DULA and DEBA: Differentiable Ergonomic Risk Models for Postural Assessment and Optimization in Ergonomically Intelligent pHRI," in *IEEE/RSJ Int. Conf. on Intelligent Robots and Systems*, 2022, pp. 9124–9131.

[16] L. Peppoloni, A. Filippeschi, E. Ruffaldi, and C. A. Avizzano, "A novel wearable system for the online assessment of risk for biomechanical load in repetitive efforts," *International Journal of Industrial Ergonomics*, vol. 52, pp. 1–11, 2016.

[17] L. Fortini, M. Lorenzini, W. Kim, E. D. Momi, and A. Ajoudani, "A Framework for Real-time and Personalisable Human Ergonomics Monitoring," *IEEE/RSJ Int. Conf. on Intel. Robots and Systems*, 2020.

[18] V. Weistroffer, F. Keith, A. Bisiaux, C. Andriot, and A. Lasnier, "Using Physics-Based Digital Twins and Extended Reality for the Safety and Ergonomics Evaluation of Cobotic Workstations," *Frontiers in Virtual Reality*, vol. 3, 2022.

[19] K. Robinette, H. Daanen, and E. Paquet, "The CAESAR project: a 3-D surface anthropometry survey," in *Second International Conference on 3-D Digital Imaging and Modeling*, 1999, pp. 380–386.

[20] P. E. Fragoso, "Introducing Multivariate Anthropometry in Digital Human Modelling," *DHM2020*, pp. 28–39, 2020.

[21] G. De Magistris, A. Micaelli, P. Evrard, C. Andriot, J. Savin, C. Gaudez, and J. Marsot, "Dynamic control of DHM for ergonomic assessments," *Int. J. of Indus. Ergonomics*, vol. 43, no. 2, 2013.

[22] A. Del Prete, N. Mansard, O. E. Ramos, O. Stasse, and F. Nori, "Implementing Torque Control with High-Ratio Gear Boxes and Without Joint-Torque Sensors," *Int. J. of Humanoid Robotics*, vol. 13, no. 1, 2016.

[23] K. Yuan, I. Chatzinikolaidis, and Z. Li, "Bayesian Optimization for Whole-Body Control of High-Degree-of-Freedom Robots Through Reduction of Dimensionality," *IEEE Rob. Autom. Let.*, vol. 4, no. 3, 2019.

[24] X. B. Peng, P. Abbeel, S. Levine, and M. Van De Panne, "DeepMimic: Example-guided deep reinforcement learning of physics-based character skills," *ACM Transactions on Graphics*, vol. 37, no. 4, pp. 1–14, 2018.

[25] J. Won and J. Lee, "Learning body shape variation in physics-based characters," *ACM Trans. on Graphics*, vol. 38, no. 6, pp. 1–12, 2019.

[26] X. Merlhiot, J. Le Garrec, G. Saupin, and C. Andriot, "The XDE mechanical kernel: Efficient and robust simulation of multibody dynamics with intermittent nonsmooth contacts," in *Proceedings of the 2nd Joint International Conference on Multibody System Dynamics*, 2012, p. 43.

[27] M. Hulens, G. Vansant, R. Lysens, A. Claessens, E. Muls, and S. Brumagne, "Study of differences in peripheral muscle strength of lean versus obese women: an allometric approach," *International Journal of Obesity*, vol. 25, no. 5, pp. 676–681, 2001.

[28] C. L. Lafortuna, N. A. Maffiuletti, F. Agosti, and A. Sartorio, "Gender variations of body composition, muscle strength and power output in morbid obesity," *Int. J. of Obesity*, vol. 29, no. 7, pp. 833–841, 2005.

[29] N. Hansen and A. Ostermeier, "Completely Derandomized Self-Adaptation in Evolution Strategies," *Evolutionary Computation*, vol. 9, no. 2, pp. 159–195, 2001.

[30] E. Dalin, I. Bergonzani, T. Anne, S. Ivaldi, and J.-B. Mouret, "Whole-body teleoperation of the Talos humanoid robot: preliminary results," in *ICRA 2021 - 5th Workshop on Teleoperation of Dynamic Legged Robots in Real Scenarios*, 2021.

IEEE Robotics and Automation Letters (RA-L) paper, presented at ICRA 2024, Yokohama, Japan. Cite as RA-L paper.